Nano Research
2022, 15(11): 9683–9688

ISSN 1998-0124 CN 11-5974/O4
https://doi.org/10.1007/s12274-022-4347-x

Research Article

Toward batch synthesis of high-quality graphene by cold-wall chemical vapor deposition approach

Kaicheng Jia[1,2,§], Ziteng Ma[1,2,§], Wendong Wang[3,§], Yongliang Wen[4,§], Huanxin Li[4,5], Yeshu Zhu[1,2,6], Jiawei Yang[7], Yuqing Song[1,2], Jiaxin Shao[1,2,6], Xiaoting Liu[1,2,6], Qi Lu[2,8], Yixuan Zhao[1,2], Jianbo Yin[2], Luzhao Sun[2], Hailin Peng[1,2], Jincan Zhang[2,5] (✉), Li Lin[9] (✉), and Zhongfan Liu[1,2] (✉)

[1] *Center for Nanochemistry, Beijing Science and Engineering Center for Nanocarbons, Beijing National Laboratory for Molecular Science, College of Chemistry and Molecular Engineering, Peking University, Beijing 100871, China*
[2] *Beijing Graphene Institute, Beijing 100095, China*
[3] *School of Physics and Astronomy, University of Manchester, Manchester M13 9PL, UK*
[4] *State Key Laboratory for Chemo/Biosensing and Chemometrics, College of Chemistry and Chemical Engineering, Hunan University, Changsha 410082, China*
[5] *Department of Engineering, University of Cambridge, Cambridge CB3 0FA, UK*
[6] *Academy for Advanced Interdisciplinary Studies, Peking University, Beijing 100871, China*
[7] *Key Laboratory of Opto-Electronics Technology, Ministry of Education, College of Electronic Science and Technology, Faculty of Information Technology, Beijing University of Technology, Beijing 100024, China*
[8] *State Key Laboratory of Heavy Oil Processing, College of Science, China University of Petroleum, Beijing 102249, China*
[9] *School of Materials Science and Engineering, Peking University, Beijing 100871, China*
[§] *Kaicheng Jia, Ziteng Ma, Wendong Wang, and Yongliang Wen contributed equally to this work.*

Received: 20 December 2021 / **Revised:** 21 March 2022 / **Accepted:** 22 March 2022

ABSTRACT

Chemical vapor deposition (CVD) has emerged as a promising approach for the controlled growth of graphene films with appealing scalability, controllability, and uniformity. However, the synthesis of high-quality graphene films still suffers from low production capacity and high energy consumption in the conventional hot-wall CVD system. In contrast, owing to the different heating mode, cold-wall CVD (CW-CVD) system exhibits promising potential for the industrial-scale production, but the quality of as-received graphene remains inferior with limited domain size and high defect density. Herein, we demonstrated an efficient method for the batch synthesis of high-quality graphene films with millimeter-sized domains based on CW-CVD system. With reduced defect density and improved properties, the as-received graphene was proven to be promising candidate material for electronics and anti-corrosion application. This study provides a new insight into the quality improvement of graphene derived from CW-CVD system, and paves a new avenue for the industrial production of high-quality graphene films for potential commercial applications.

KEYWORDS

graphene, cold-wall chemical vapor deposition (CVD), defects, electrical performance

1 Introduction

Chemical vapor deposition (CVD) has been proven to be an appealing approach for the industrial production of graphene films with superior controllability and uniformity [1, 2]. The past few years have witnessed significant progress in the quality improvement of CVD-derived graphene, gradually narrowing the gap to the promising quality of its mechanically exfoliated counterpart [3–6]. However, the synthesis of high-quality graphene films is still mainly in the laboratory scale with low production capacity and efficiency, strongly hindering its downstream applications especially in commercial fields [7, 8]. To solve this, academic efforts have been devoted to developing scalable growth technologies and equipments [9]. Currently, this issue remains unresolved as reflected by the level of reported domain size and carrier mobility of graphene samples acquired from scalable production [10–14].

Based on the different heating modes, CVD system can be divided into how-wall CVD (HW-CVD) and cold-wall CVD (CW-CVD) system [15]. Instead of heating from the outer wall of the reaction chamber in HW-CVD system, thermal energy is concentrated on the growth substrate of graphene in CW-CVD system; therefore, the chamber wall would remain at relatively low temperature, which would save the heating time [16]. In this case, the production efficiency of CW-CVD system would be enhanced owing to the improved energy efficiency and saved time for heating [17]. Besides, in CW-CVD system, the sample size of graphene films can be potentially enlarged to over meter scale in both length and width, beyond the reach of quartz tube, commonly used as the reaction chamber in HW-CVD system.

Address correspondence to Jincan Zhang, zhangjc-cnc@pku.edu.cn; Li Lin, linli-cnc@pku.edu.cn; Zhongfan Liu, zfliu@pku.edu.cn

However, two factors, the high defect density and small domain size of the graphene grown in CW-CVD system make its quality not comparable to that of graphene grown in how-wall CVD system [18, 19]. In this regard, a facile and scalable method to grow high-quality graphene films in CW-CVD system still requires critical efforts.

Herein, we developed an efficient method for the batch synthesis of graphene films with millimeter-sized domains in CW-CVD system. The improved domain size was mainly attributed to the formation of confined space using graphite susceptor and reduced carbon feedstock supply. To further improve the quality of graphene films derived from CW-CVD system, "etching-regrowth" strategy was developed to reduce the defect density of graphene. Owing to the improved quality, graphene grown from CW-CVD system exhibited appealing electrical properties and promising potentials for applications such as electronics and anti-corrosion.

2 Results and discussion

Grain boundaries are line defects formed when two adjacent graphene domains with different orientations merges, which would highly degrade the properties of graphene [20, 21]. The domain size of CW-CVD graphene is commonly in the range of tens of micrometers, which means the density of grain boundaries in final graphene films is extremely high [19, 22, 23]. To grow large graphene single crystals, reduction of the nucleation density is an efficient approach. In the conventional CW-CVD system, carbon feedstock is introduced from the showerhead above the Cu foil to initiate graphene growth. This mass transport mode would result in an inhomogeneous distribution of gas flow and relatively high concentration of carbon species above the Cu surface (Fig. S1 in the Electronic Supplementary Material (ESM)). To solve this, graphite susceptor was utilized to build a spatially confined space, which would alter the dynamics of gas flow. Figure 1(a) illustrates the schematic of the batch synthesis of large graphene single crystals in CW-CVD system with confined growth spaces. As confirmed by the computational fluid dynamics (CFD) simulation results, owing to the space confinement introduced by the stacking of the susceptor, only small proportion of carbon feedstock would enter into the confined spaces in the lateral direction with decreased velocity; therefore, the concentration of carbon species above the surface of Cu substrates for graphene nucleation would be dramatically reduced (Figs. 1(b) and 1(c), and Fig. S2 in the ESM). Besides, the distribution of the velocity of gas flow inside the confined space between two adjacent susceptor was more uniform than that above the susceptor, which would contribute to improving the homogeneity of as-obtained graphene films (Fig. S3 in the ESM). With the assistance of the graphite susceptor, 5 pieces of large-area graphene films (0.1 m × 0.1 m) can be grown at the same time with domain size increased to sub-millimeter level (Figs. 1(d) and 1(e), and Figs. S4 and S5 in the ESM). The statistics of graphene domain size from pieces numbered 1–5 confirmed the high uniformity among different graphene films (Fig. 1(f)). Raman characterization was conducted to probe the quality of as-received graphene films, and the noise level of D peak intensity from graphene on Cu suggested the improved crystallinity of graphene (Fig. S6 in the ESM) [24]. With optimized nucleation conditions such as extending Ar annealing time of Cu substrate, millimeter-sized graphene single crystals can be obtained in CW-CVD system (Fig. S7 in the ESM).

Besides grain boundaries, point defect is another defective structure commonly existing in graphene films derived from CW-CVD system [23, 25, 26]. To exclude the interference from grain boundaries and transfer-induced breakages on the evaluation of the density of point defects, the region for Raman characterization was carefully selected within a single-crystal domain of intact graphene transferred on SiO_2/Si substrate. Specifically, Raman mapping of the ratio of the D band and G band intensity (I_D/I_G) was conducted to visualize the spatial distribution of point defects. Random distribution of the probed region with high I_D/I_G was observed, indicating the presence of dense point defects originated from CVD growth [27]. In detail, only about 50% region in the Raman mapping exhibited the level of I_D/I_G value less than 0.02, while about 40% region indicated the I_D/I_G of 0.02–0.04 and I_D/I_G of remaining region even reached 0.1, according to the statistical results (Fig. S8 in the ESM).

To further reduce the defect density in CW-CVD graphene, "etching-regrowth" strategy was developed relying on the difference of etching activity between point defects and intact

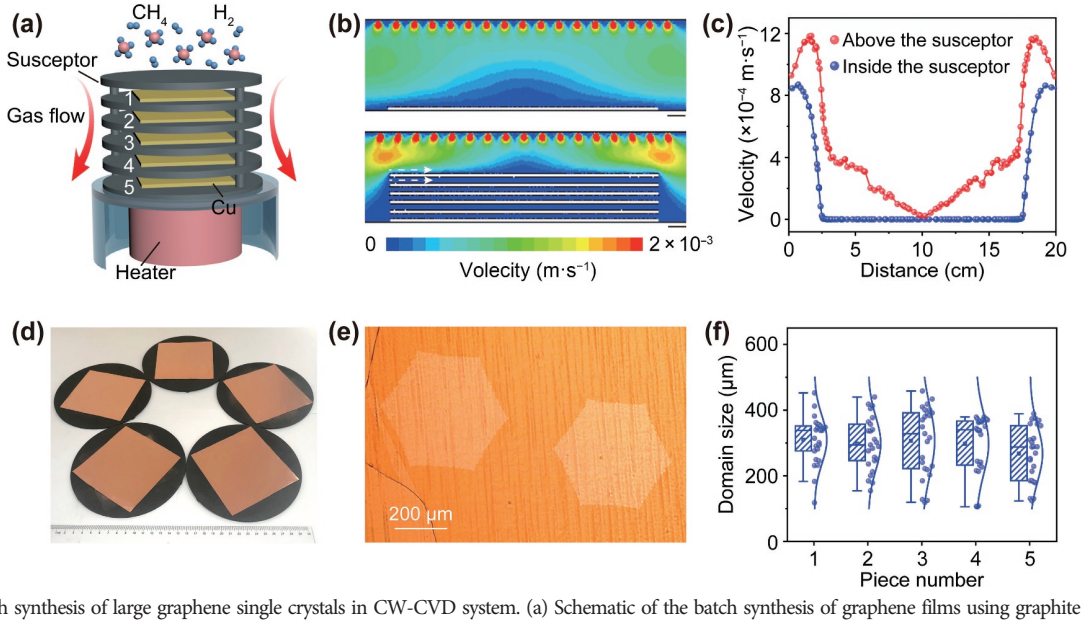

Figure 1 Batch synthesis of large graphene single crystals in CW-CVD system. (a) Schematic of the batch synthesis of graphene films using graphite susceptor. (b) CFD simulation results of the velocity distribution of gas flow without (up) and with (down) susceptor. Scale bar: 1 cm. (c) Velocity profiles along the white dashed arrow marked in (b). (d) Photograph of 5 pieces of 0.1 m × 0.1 m-sized CW-CVD graphene on Cu substrates. (e) Optical microscopy (OM) image of as-received graphene single crystals. (f) Statistics of the domain size of CW-CVD graphene from different pieces as illustrated in (a).

graphene lattice. Figure 2(a) illustrates the process of "etching-regrowth", in which H_2 was introduced into the chamber after graphene growth to initiate the etching of the defects. Subsequently, CH_4 was introduced again for the regrowth of the etched region; therefore, the density of defects could be reduced. After optimizing the conditions of H_2 etching, specifically the gas flow and etching time of H_2 (Figs. 2(b) and 2(c), and Figs. S9 and S10 in the ESM), high-quality graphene films with decreased defect density could be obtained. Based on the statistics of over 1500 region from Raman mapping results, the percentage of probed region with I_D/I_G value less than 0.02 could increase to around 90%, consistent with the uniform contrast in Raman mapping results (Fig. 2(d)). To evaluate the quality of graphene films with and without "etching-regrowth" treatment over a large scale, graphene films were transferred onto 4-inch SiO_2/Si wafers and subsequently characterized by large-area Raman mapping with the length of the detected region reaching 0.2 mm (Fig. 2(e)). The obvious reduction of the defect density of graphene with "etching-regrowth" treatment was further confirmed by the reduced D band intensity over large area (Figs. 2(f) and 2(g)).

To further evaluate the electrical properties of as-obtained CW-CVD graphene, Hall-bar devices were fabricated based on the encapsulated graphene by two flakes of hexagonal boron nitride (hBN), which would exclude the scattering from the substrate [28]. Figure 3(a) demonstrated a representative Raman spectrum of graphene sandwiched in hBN, where the high intensity ratio of 2D band and G band (~ 6.6) and low value of full width at half maximum (FWHM) of the 2D band (~ 18.8 cm^{-1}) indicated the high quality and reduced doping level of grown graphene [29]. Typical transfer curve measured at room temperature was shown in Fig. 3(b), and the mobility of graphene could be extracted by plotting the conductivity as a function of charge carrier concentration (Fig. S11 in the ESM). Remarkably, the room-temperature carrier mobilities were 7.3 × 10^4 and 8.3 × 10^4 $cm^2 \cdot V^{-1} \cdot s^{-1}$ for holes and electrons, respectively. These carrier mobility values of the as-received graphene are higher than previously reported results for CW-CVD graphene [30, 31], and comparable to those of HW-CVD and mechanically exfoliated counterpart. Besides, low-temperature Hall measurements were also conducted to investigate the electronic quality of graphene. Temperature-dependence of as-obtained Hall mobility of graphene was presented in Fig. 3(c), in which the value of Hall mobility could reach about 3 × 10^5 $cm^2 \cdot V^{-1} \cdot s^{-1}$ at 1.8 K. Note that Shubnikov-de Haas (SdH) oscillations of longitudinal resistance could be observed at magnetic field as low as 0.1 T, also indicating a high electronic quality of graphene [32]. Additionally, sheet resistance of graphene with and without "etching-regrowth" treatment was measured by using a four-probe configuration, respectively. Graphene with "etching-regrowth" treatment exhibited reduced sheet resistance with a narrow distribution, as confirmed by the statistics and mapping results of sheet resistance in Fig. 3(d). Above measurement results altogether confirmed the improved quality of graphene by our "etching-regrowth" strategy [33], indicating its promising potential for applications in high-performance electronics in the future.

Because of the decreased density of defects, as-obtained high-quality CW-CVD graphene exhibited promising potential for the anti-corrosion of Cu. Specifically, point defects and grain boundaries would degrade the intrinsic impermeability of graphene, and the defects would also serve as diffusion channels for corrosive fluids onto Cu surface, which would accelerate the electrochemical corrosion [34, 35]. It should be noted that, to exclude the interference from the Cu crystallographic orientations and their interaction with graphene on the corrosion [36], Cu(111) foil obtained from annealing and graphene films grown on Cu(111) surface were selected for anti-corrosion experiment (Fig. S12 in the ESM). To evaluate the anti-corrosion capacity of graphene with and without "etching-regrowth" treatment, electrochemical measurement was conducted with NaCl solution (3.5%) as electrolyte, as illustrated in Fig. 4(a). Figure 4(b)

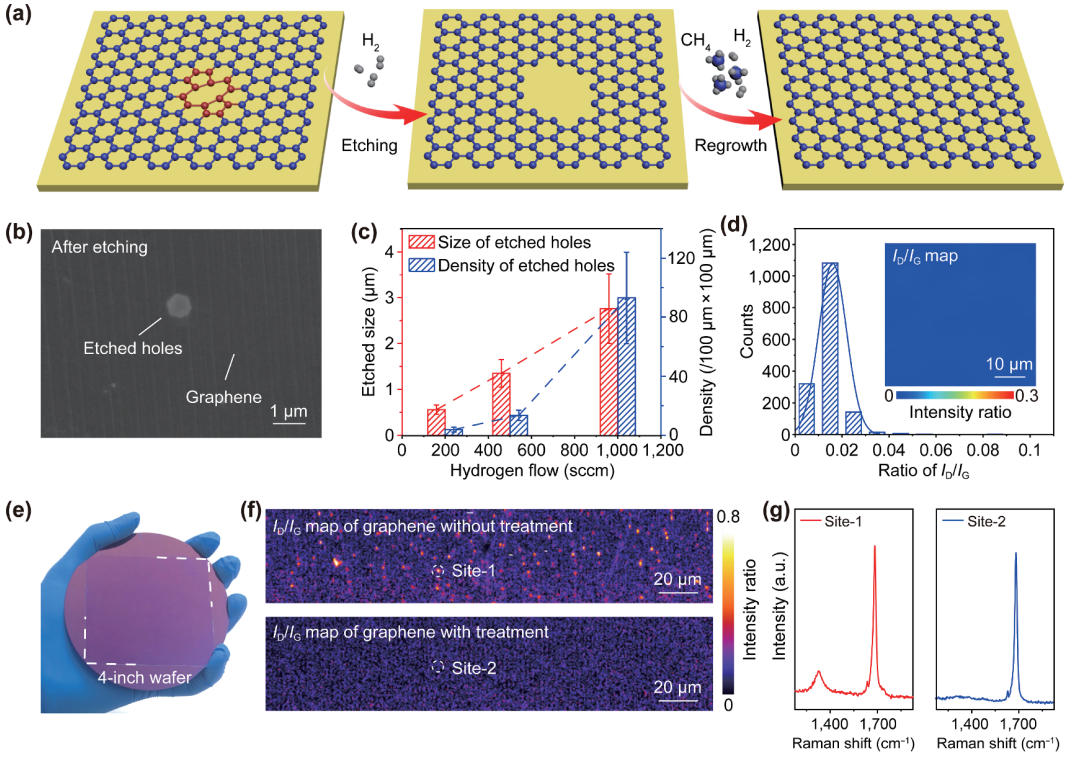

Figure 2 Elimination of the defects by "etching-regrowth" treatment. (a) Schematic of the "etching-regrowth" process. (b) Typical SEM image of graphene after H_2 etching. (c) Statistics of the size and density of etched holes of graphene after H_2 etching. (d) Statistics of I_D/I_G of graphene with "etching-regrowth" treatment. Inset: I_D/I_G mapping results. (e) Photograph of graphene film transferred on a 4-inch SiO_2/Si wafer. (f) I_D/I_G mapping results of graphene without (up) and with (down) "etching-regrowth" treatment. (g) Corresponding Raman spectra of graphene marked in (f).

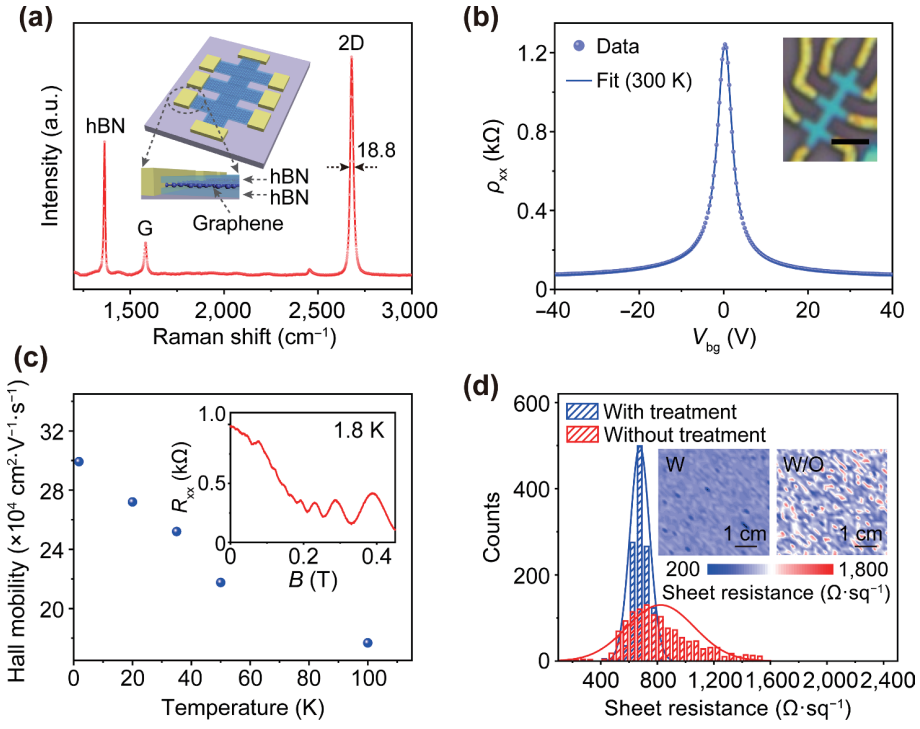

Figure 3 Electrical properties of CW-CVD graphene. (a) Raman spectrum of graphene encapsulated by hBN. Inset: Schematic of the Hall-bar device. (b) Typical plot of the longitude resistivity (ρ_{xx}) as a function of back-gate voltage (V_{bg}) at room temperature. Inset: OM image of the measured Hall-bar device. Scale bar: 2 μm. (c) Temperature-dependence of Hall mobilities. Inset: Longitude resistance (R_{xx}) as a function of magnetic field (B) at 1.8 K. (d) Statistics of sheet resistance of CW-CVD graphene. Inset: Sheet resistance mapping of CW-CVD graphene with (left) and without treatment (right).

demonstrates the Tafel polarization curves measured in the first day, from which both graphene with and without "etching-regrowth" treatment exhibited improved anti-corrosion performance. However, about one order of magnitude reduction in corrosion current density than Cu confirmed the superior anti-corrosion capacity contributed by the improved quality of graphene with "etching-regrowth" treatment [37]. Besides, electrochemical impedance spectroscopy (EIS) was also conducted to further evaluate the anti-corrosion performance [38]. The semicircle diameter of graphene without the treatment is larger than that of Cu, but smaller than that of graphene with the treatment, indicating the degradation of anti-corrosion properties originated from the presence of graphene defects (Fig. 4(c)). Notably, the measured corrosion current density of graphene with the treatment exhibited almost no changes after one week's electrochemical measurement. In contrast, the corrosion current density of graphene without the treatment quickly increased to the level of Cu without the coating of graphene, indicating that graphene with dense defects could only protect underlying Cu at early stage and fail in long term perspective (Fig. 4(d) and Fig. S13 in the ESM). Scanning electron microscopy (SEM) and atomic force microscopy (AFM) characterization were carried out to investigate the surface morphology of the samples after electrochemical test. Obvious Cu corrosion with pitting

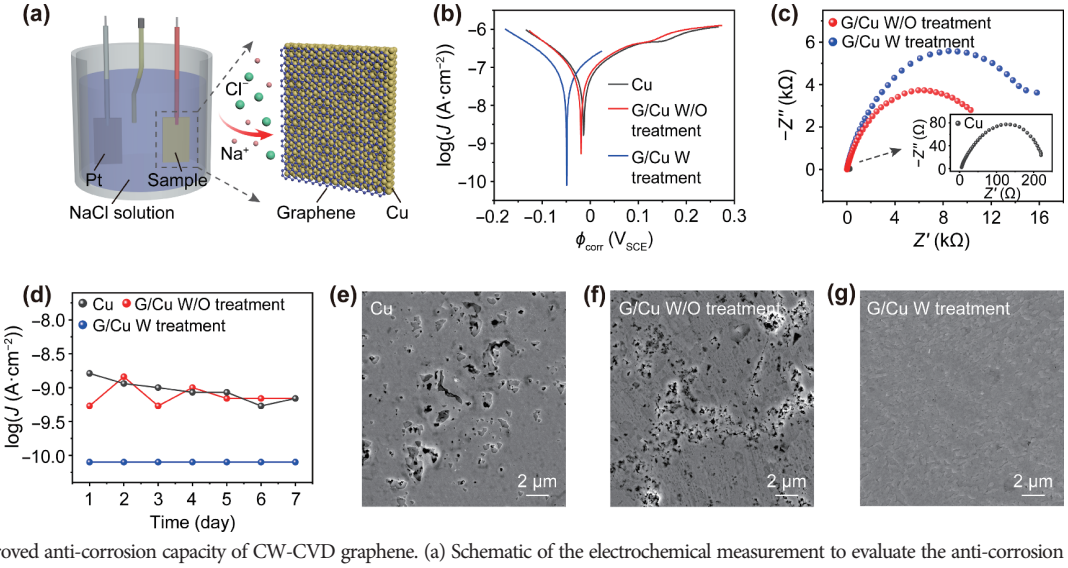

Figure 4 Improved anti-corrosion capacity of CW-CVD graphene. (a) Schematic of the electrochemical measurement to evaluate the anti-corrosion performance of graphene. (b) Tafel polarization curves of Cu (black), graphene/Cu without the treatment (W/O treatment) (red), and graphene/Cu with the treatment (W treatment) (blue), respectively. (c) EIS curves of Cu (black), graphene/Cu without the treatment (red), and graphene/Cu with the treatment (blue), respectively. (d) Statistics of the corrosion current density during one week's measurement. SEM images of Cu (e), graphene/Cu without the treatment (f), and graphene/Cu with the treatment (g) after electrochemical measurement.

morphology was observed on both Cu and graphene/Cu without the treatment after the electrochemical measurement, while on the graphene/Cu surface with the treatment, nearly no corrosion was observed, consistent with the electrochemical results (Figs. 4(e)–4(g) and Figs. S14 and S15 in the ESM).

3 Conclusions

In conclusion, we demonstrated a facile approach for the batch synthesis of high-quality graphene films in CW-CVD system. With the assistance of graphite susceptor to alter the dynamics of gas flow, the graphene nucleation density was efficiently reduced and thus millimeter-scale single crystals were successfully obtained in CW-CVD system. Moreover, "etching-regrowth" strategy was applied to further reduce the defect density in as-obtained graphene, ensuring the improved electrical properties such as high carrier mobility and uniform sheet resistance. Furthermore, CW-CVD graphene after removal of the defects was also proven to be a promising material for the anti-corrosion of Cu. This study provides a new insight into the quality improvement of CW-CVD derived graphene, and paves a new avenue for the large-scale production of graphene films with promising properties for future applications.

Acknowledgements

This work was financially supported by the National Natural Science Foundation of China (Nos. T2188101, 21525310, and 52072042), the National Key R&D Program of China (No. 2018YFA0703502), Beijing National Laboratory for Molecular Sciences (No. BNLMS-CXTD-202001), and Beijing Municipal Science & Technology Commission (Nos. Z181100004818001, Z18110300480001, Z18110300480002, Z191100000819005, Z191100000819007, and Z201100008720005).

Electronic Supplementary Material: Supplementary material (further details of experiment, TEM measurements, and so on) is available in the online version of this article at https://doi.org/10.1007/s12274-022-4347-x.

References

[1] Lin, L.; Deng, B.; Sun, J. Y.; Peng, H. L.; Liu, Z. F. Bridging the gap between reality and ideal in chemical vapor deposition growth of graphene. *Chem. Rev.* **2018**, *118*, 9281–9343.

[2] Novoselov, K. S.; Fal'ko, V. I.; Colombo, L.; Gellert, P. R.; Schwab, M. G.; Kim, K. A roadmap for graphene. *Nature* **2012**, *490*, 192–200.

[3] Hao, Y. F.; Bharathi, M. S.; Wang, L.; Liu, Y. Y.; Chen, H.; Nie, S.; Wang, X. H.; Chou, H.; Tan, C.; Fallahazad, B. et al. The role of surface oxygen in the growth of large single-crystal graphene on copper. *Science* **2013**, *342*, 720–723.

[4] Lin, L.; Zhang, J. C.; Su, H. S.; Li, J. Y.; Sun, L. Z.; Wang, Z. H.; Xu, F.; Liu, C.; Lopatin, S.; Zhu, Y. H. et al. Towards super-clean graphene. *Nat. Commun.* **2019**, *10*, 1912.

[5] Zhang, J. C.; Sun, L. Z.; Jia, K. C.; Liu, X. T.; Cheng, T.; Peng, H. L.; Lin, L.; Liu, Z. F. New growth frontier: Superclean graphene. *ACS Nano* **2020**, *14*, 10796–10803.

[6] Yuan, G. W.; Lin, D. J.; Wang, Y.; Huang, X. L.; Chen, W.; Xie, X. D.; Zong, J. Y.; Yuan, Q. Q.; Zheng, H.; Wang, D. et al. Proton-assisted growth of ultra-flat graphene films. *Nature* **2020**, *577*, 204–208.

[7] Kong, W.; Kum, H.; Bae, S. H.; Shim, J.; Kim, H.; Kong, L. P.; Meng, Y.; Wang, K. J.; Kim, C.; Kim, J. Path towards graphene commercialization from lab to market. *Nat. Nanotechnol.* **2019**, *14*, 927–938.

[8] Jia, K. C.; Zhang, J. C.; Zhu, Y. S.; Sun, L. Z.; Lin, L.; Liu, Z. F. Toward the commercialization of chemical vapor deposition graphene films. *Appl. Phys. Rev.* **2021**, *8*, 041306.

[9] Lin, L.; Peng, H. L.; Liu, Z. F. Synthesis challenges for graphene industry. *Nat. Mater.* **2019**, *18*, 520–524.

[10] Bae, S.; Kim, H.; Lee, Y.; Xu, X. F.; Park, J. S.; Zheng, Y.; Balakrishnan, J.; Lei, T.; Kim, H. R.; Song, Y. I. et al. Roll-to-roll production of 30-inch graphene films for transparent electrodes. *Nat. Nanotechnol.* **2010**, *5*, 574–578.

[11] Xu, J. B.; Hu, J. X.; Li, Q.; Wang, R. B.; Li, W. W.; Guo, Y. F.; Zhu, Y. B.; Liu, F. K.; Ullah, Z.; Dong, G. C. et al. Fast batch production of high-quality graphene films in a sealed thermal molecular movement system. *Small* **2017**, *13*, 1700651.

[12] Zhang, Y. N.; Huang, D. P.; Duan, Y. W.; Chen, H.; Tang, L. L.; Shi, M. Q.; Li, Z. C.; Shi, H. F. Batch production of uniform graphene films via controlling gas-phase dynamics in confined space. *Nanotechnology* **2021**, *32*, 105603.

[13] Jo, I.; Park, S.; Kim, D.; Moon, J. S.; Park, W. B.; Kim, T. H.; Kang, J. H.; Lee, W.; Kim, Y.; Lee, D. N. et al. Tension-controlled single-crystallization of copper foils for roll-to-roll synthesis of high-quality graphene films. *2D Mater.* **2018**, *5*, 024002.

[14] Kobayashi, T.; Bando, M.; Kimura, N.; Shimizu, K.; Kadono, K.; Umezu, N.; Miyahara, K.; Hayazaki, S.; Nagai, S.; Mizuguchi, Y. at al. Production of a 100-m-long high-quality graphene transparent conductive film by roll-to-roll chemical vapor deposition and transfer process. *Appl. Phys. Lett.* **2013**, *102*, 023112.

[15] Sun, L. Z.; Yuan, G. W.; Gao, L. B.; Yang, J.; Chhowalla, M.; Gharahcheshmeh, M. H.; Gleason, K. K.; Choi, Y. S.; Hong, B. H.; Liu, Z. F. Chemical vapour deposition. *Nat. Rev. Methods Primers* **2021**, *1*, 5.

[16] Jia, K. C.; Ci, H. N.; Zhang, J. C.; Sun, Z. T.; Ma, Z. T.; Zhu, Y. S.; Liu, S. N.; Liu, J. L.; Sun, L. Z.; Liu, X. T. et al. Superclean growth of graphene using a cold-wall chemical vapor deposition approach. *Angew. Chem., Int. Ed.* **2020**, *59*, 17214–17218.

[17] Kim, S. M.; Kim, J. H.; Kim, K. S.; Hwangbo, Y.; Yoon, J. H.; Lee, E. K.; Ryu, J.; Lee, H. J.; Cho, S.; Lee, S. M. Synthesis of CVD-graphene on rapidly heated copper foils. *Nanoscale* **2014**, *6*, 4728–4734.

[18] Alnuaimi, A.; Almansouri, I.; Saadat, I.; Nayfeh, A. Toward fast growth of large area high quality graphene using a cold-wall CVD reactor. *RSC Adv.* **2017**, *7*, 51951–51957.

[19] Bointon, T. H.; Barnes, M. D.; Russo, S.; Craciun, M. F. High quality monolayer graphene synthesized by resistive heating cold wall chemical vapor deposition. *Adv. Mater.* **2015**, *27*, 4200–4206.

[20] Huang, P. Y.; Ruiz-Vargas, C. S.; van der Zande, A. M.; Whitney, W. S.; Levendorf, M. P.; Kevek, J. W.; Garg, S.; Alden, J. S.; Hustedt, C. J.; Zhu, Y. et al. Grains and grain boundaries in single-layer graphene atomic patchwork quilts. *Nature* **2011**, *469*, 389–392.

[21] Ma, T.; Liu, Z. B.; Wen, J. X.; Gao, Y.; Ren, X. B.; Chen, H. J.; Jin, C. H.; Ma, X. L.; Xu, N. S.; Cheng, H. M. et al. Tailoring the thermal and electrical transport properties of graphene films by grain size engineering. *Nat. Commun.* **2017**, *8*, 14486.

[22] Ryu, J.; Kim, Y.; Won, D.; Kim, N.; Park, J. S.; Lee, E. K.; Cho, D.; Cho, S. P.; Kim, S. J.; Ryu, G. H. et al. Fast synthesis of high-performance graphene films by hydrogen-free rapid thermal chemical vapor deposition. *ACS Nano* **2014**, *8*, 950–956.

[23] Luo, B. R.; Whelan, P. R.; Shivayogimath, A.; Mackenzie, D. M. A.; Bøggild, P.; Booth, T. J. Copper oxidation through nucleation sites of chemical vapor deposited graphene. *Chem. Mater.* **2016**, *28*, 3789–3795.

[24] Ferrari, A. C.; Basko, D. M. Raman spectroscopy as a versatile tool for studying the properties of graphene. *Nat. Nanotechnol.* **2013**, *8*, 235–246.

[25] Shah, S.; Chiou, Y. C.; Lai, C. Y.; Apostoleris, H.; Rahman, M.; Younes, H.; Almansouri, I.; Al Ghaferi, A.; Chiesa, M. Impact of short duration, high-flow H_2 annealing on graphene synthesis and surface morphology with high spatial resolution assessment of coverage. *Carbon* **2017**, *125*, 318–326.

[26] Arjmandi-Tash, H.; Lebedev, N.; van Deursen, P. M. G.; Aarts, J.; Schneider, G. F. Hybrid cold and hot-wall reaction chamber for the rapid synthesis of uniform graphene. *Carbon* **2017**, *118*, 438–442.

[27] Cançado, L. G.; Jorio, A.; Ferreira, E. H. M.; Stavale, F.; Achete, C. A.; Capaz, R. B.; Moutinho, M. V. O.; Lombardo, A.; Kulmala, T. S.; Ferrari, A. C. Quantifying defects in graphene via Raman

spectroscopy at different excitation energies. *Nano Lett.* **2011**, *11*, 3190–3196.

[28] Dean, C. R.; Young, A. F.; Meric, I.; Lee, C.; Wang, L.; Sorgenfrei, S.; Watanabe, K.; Taniguchi, T.; Kim, P.; Shepard, K. L. et al. Boron nitride substrates for high-quality graphene electronics. *Nat. Nanotechnol.* **2010**, *5*, 722–726.

[29] Lee, J. E.; Ahn, G.; Shim, J.; Lee, Y. S.; Ryu, S. Optical separation of mechanical strain from charge doping in graphene. *Nat. Commun.* **2012**, *3*, 1024.

[30] Piner, R.; Li, H. F.; Kong, X. H.; Tao, L.; Kholmanov, I. N.; Ji, H. X.; Lee, W. H.; Suk, J. W.; Ye, J.; Hao, Y. F. et al. Graphene synthesis via magnetic inductive heating of copper substrates. *ACS Nano* **2013**, *7*, 7495–7499.

[31] Miseikis, V.; Bianco, F.; David, J.; Gemmi, M.; Pellegrini, V.; Romagnoli, M.; Coletti, C. Deterministic patterned growth of high-mobility large-crystal graphene: A path towards wafer scale integration. *2D Mater.* **2017**, *4*, 021004.

[32] Lin, L.; Li, J. Y.; Ren, H. Y.; Koh, A. L.; Kang, N.; Peng, H. L.; Xu, H. Q.; Liu, Z. F. Surface engineering of copper foils for growing centimeter-sized single-crystalline graphene. *ACS Nano* **2016**, *10*, 2922–2929.

[33] Banszerus, L.; Schmitz, M.; Engels, S.; Dauber, J.; Oellers, M.; Haupt, F.; Watanabe, K.; Taniguchi, T.; Beschoten, B.; Stampfer, C. Ultrahigh-mobility graphene devices from chemical vapor deposition on reusable copper. *Sci. Adv.* **2015**, *1*, e1500222.

[34] Zhao, Z. J.; Hou, T. Y.; Wu, N. N.; Jiao, S. P.; Zhou, K.; Yin, J.; Suk, J. W.; Cui, X.; Zhang, M. F.; Li, S. P. et al. Polycrystalline few-layer graphene as a durable anticorrosion film for copper. *Nano Lett.* **2021**, *21*, 1161–1168.

[35] Chang, C.; Chen, W.; Chen, Y.; Chen, Y. H.; Chen, Y.; Ding, F.; Fan, C. H.; Fan, H. J.; Fan, Z. X.; Gong, C. et al. Recent progress on two-dimensional materials. *Acta Phys. Chim. Sin.* **2021**, *37*, 2108017.

[36] Xu, X. Z.; Yi, D.; Wang, Z. C.; Yu, J. C.; Zhang, Z. H.; Qiao, R. X.; Sun, Z. H.; Hu, Z. H.; Gao, P.; Peng, H. L. et al. Greatly enhanced anticorrosion of Cu by commensurate graphene coating. *Adv. Mater.* **2018**, *30*, 1702944.

[37] Kirkland, N. T.; Schiller, T.; Medhekar, N.; Birbilis, N. Exploring graphene as a corrosion protection barrier. *Corros. Sci.* **2012**, *56*, 1–4.

[38] Ye, X. H.; Lin, Z.; Zhang, H. J.; Zhu, H. W.; Liu, Z.; Zhong, M. L. Protecting carbon steel from corrosion by laser *in situ* grown graphene films. *Carbon* **2015**, *94*, 326–334.